Above-barrier states in In$_x$Ga$_{1-x}$As/GaAs multiple quantum wells with a thin cap layer

T. Worren,* K. B. Ozanyan,† and O. Hunderi

Department of Physics, Norwegian University of Science and Technology, N-7034 Trondheim, Norway

F. Martelli

Fondazione Ugo Bordoni, via Baldassarre Castiglione 59, I-00142 Roma, Italy

The effective-mass approximation in a transfer-matrix formalism is used to investigate above-barrier states in strained In$_x$Ga$_{1-x}$As/GaAs multiple quantum wells (MQW's). A condition for finding above-barrier states, semiconfined by a finite cap layer, is formulated. In the derivation of the transfer matrices, boundary conditions that include the discontinuity of the lattice constant in the growth direction are used. In a series of In$_x$Ga$_{1-x}$As/GaAs MQW's (4–6 periods, $x \simeq 0.1$, with the topmost barrier used as a cap) the energies of the light-hole and heavy-hole excitonic peaks, involving both above-barrier and confined states, are observed by photoluminescence excitation spectroscopy (PLE) and polarized PLE. The experimental values are in very good agreement with the calculated ones, for transitions involving above-barrier as well as confined states, supporting the validity of our calculations. [S0163-1829(98)11331-0]

I. INTRODUCTION

Above-barrier states in semiconductor multiple quantum wells (MQW's) and superlattices (SL's) have received increasing attention in the last decade.[1–14] Optical transitions involving above-barrier states in GaAs/Al$_{1-x}$Ga$_x$As were first studied by Zucker *et al.*[1] using resonant Raman scattering (RRS) and by Bastard *et al.*[2] using photoluminescence excitation spectroscopy (PLE). The first observations of unconfined features in the In$_x$Ga$_{1-x}$As/GaAs system were reported by Pan *et al.* in Ref. 8 and in the Zn$_{1-x}$Cd$_x$Se/Zn$_{1-x}$Mn$_x$Se system by Zhang *et al.* in Ref. 11. The latter used magnetoabsorption measurements to detect the above-barrier states, and they found that the above-barrier excitons were localized in the barrier regions. Exciton confinement in the barriers was found for In$_x$Ga$_{1-x}$As/GaAs MQW's by Martelli *et al.*[12] and Capizzi *et al.*[13]

Transitions involving above-barrier states have been treated theoretically by means of a pseudopotential method by Wong *et al.*,[3] a two-band tight-binding model in Refs. 4 and 5 and an envelope function model in Refs. 2 and 7–10. It has been shown that the intensity of the transition between the first unconfined conduction- and valence-band states depends on the barrier width[4] and that the unconfined states shift to lower energies as the barrier width increases.[6,10,12,13] Recently Wen *et al.*[14] presented a theory for above-barrier excitons in semiconductor SL's, accounting for the valence-band mixing, excitonic effects, and Fano resonances. This theory does not include strain, and is therefore not directly applicable for In$_x$Ga$_{1-x}$As/GaAs structures. Strain has been included in the numerical solutions of the complete **k·p** Hamiltonian for confined states in SL's by Jogai and Yu.[15] Although they obtain good agreement with the measurements of a series of In$_x$Ga$_{1-x}$As/GaAs MQW's, such MQW's with few periods (2–20) cannot be treated as SL's since periodic boundary conditions cannot be assumed in this case. Other groups[8,10,16,17] have used simplified versions of Kane's complete **k·p** model to calculate the confined energy levels, also in good agreement with experiment.

Calculation of above-barrier states in strained MQW structures with few periods and a finite cap layer width has, to our knowledge, not been performed yet. We therefore develop in this paper a transfer-matrix formulation of the envelope wave-function approximation to calculate envelope functions and energy levels for confined and above-barrier (semiconfined) electronic states in In$_x$Ga$_{1-x}$As/GaAs MQW's. The transfer-matrix formalism has been used by several groups (see, for example, Refs. 18 and 19) to investigate confined states in quantum structures, and has proven to give good agreement between theory and experiments, but it has not yet been applied to above-barrier states. The transfer-matrix method we present is applicable for confined and above-barrier states in a large variety of sample structures, that may incorporate strain. We also show the sensitivity of the above-barrier states to sample parameters, such as layer widths, well depths, number of periods, and the height of the vacuum potential.

Furthermore we have performed PLE measurements on a series of samples with various well and barrier widths determined, together with the indium content, using x-ray diffraction. To distinguish between transitions involving light holes and heavy holes we performed polarized PLE on some of the samples. We also calculated the overlap integral for the electron and hole envelope functions to aid the interpretation of the PLE spectra.

Section II presents the transfer-matrix formalism adapted to our sample structures. The samples and experiments are described in Sec. III. The experimental and theoretical results are presented in Secs. IV and V, respectively. Section VI contains the discussion and finally Sec. VII summarizes and concludes the work. The Appendix contains the details of the derivation of the transfer matrices and the procedure to obtain the energy levels in a MQW.
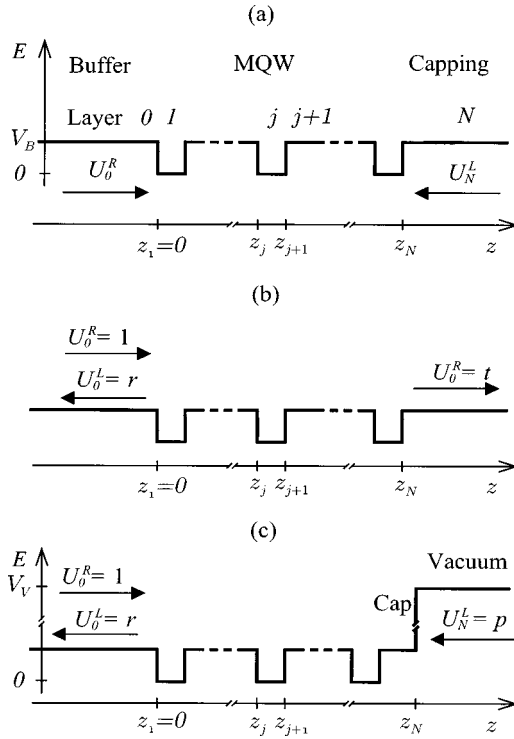
FIG. 1. Potential profile (thick line) of a typical sample structure with infinite [(a) and (b)] and finite (c) cap-layer width. The structure in (a) and (b) has $N+1$ layers including buffer and capping, and in (c) $N+1$ layers including buffer, capping, and vacuum. V_j is the potential in layer j and all energies are measured from the bottom of the wells, where $V=0$. Also shown in the figure (arrows with closed heads) are the components of the envelope wave functions in the zeroth and the Nth layers for confined (a), unconfined (b), and semiconfined above-barrier (c) states.

II. THEORY

A. Method

The transfer-matrix formalism[20] is not new in quantum mechanics and has been used to solve the one-dimensional Schrödinger equation for quantum structures, see, for example, Refs. 18 and 19. We apply the transfer-matrix formalism to a one-band envelope function approximation. Different notations and definitions of the transfer matrices used by different groups lead to the necessity of explicitly writing out the definitions and notations used in this paper. The details in the derivation and the use of the transfer matrices are given in the Appendix.

1. Definitions

The electrostatic potential profile of a typical MQW structure is shown in Fig. 1(a). In realistic samples the cap layer is of finite width and a potential profile such as the one in Fig. 1(c) should be used. For a piecewise constant potential with finite steps, the envelope wave function[21] of a carrier can be expressed as

$$\psi_j = U_j^R \exp[k_j (z-z_j)] + U_j^L \exp[-k_j(z-z_j)]. \quad (2.1)$$

Here U_j^R and U_j^L are the amplitudes of the right and left ''propagating'' components, respectively. [The time-independent wave function ψ in Eq. (2.1) must be multiplied

by $e^{-i\omega t}$ to really propagate.] They can be treated as the components of the amplitude vector of layer j

$$\mathbf{U}_j = \begin{bmatrix} U_j^R \\ U_j^L \end{bmatrix}. \quad (2.2)$$

k_j is defined as

$$k_j = \frac{\sqrt{2 \cdot m_j^*(V_j - E)}}{\hbar}, \quad (2.3)$$

where m_j^* and V_j are the effective mass (from here on we drop the asterisk $*$ to simplify the notation) and the potential in the layer j, respectively, and E is the particle's energy measured from the bottom of the well. The well layers are defined to have $V_j = 0$ and for the barriers $V_j = V_B$. If a charge carrier in layer j has energy larger than the potential V_j, then k_j is imaginary and the charge carrier is propagating (in layer j). If E is smaller than V_j then k_j is real and the particle is exponentially damped in layer j. If E is larger than the largest V_j, the particle is propagating in the whole of the structure: it is unconfined.

The standard BenDaniel-Duke boundary conditions ($\psi=$ continuous and $(1/m)(d\psi/dz)=$ continuous) can be applied by defining a state vector

$$\chi_j(z) = \begin{bmatrix} \psi_j(z) \\ \dfrac{1}{m_j}\dfrac{d}{dz}\psi_j(z) \end{bmatrix}. \quad (2.4)$$

Then the condition for smooth joining at the interface at z_{j+1} between the layers j and $j+1$ has the form

$$\chi_j(z_{j+1}) = \chi_{j+1}(z_{j+1}). \quad (2.5)$$

Einevoll and Sham show in Ref. 22 that for strained heterostructures, i.e., at interfaces between materials with dissimilar band-edge Bloch functions, the boundary conditions for conduction-band envelope functions are different from the BenDaniel-Duke conditions. The lattice constant enters the boundary conditions when the Bloch functions are assumed to have a node at the matching points.[22] If the Bloch functions have maxima at the matching points the BenDaniel-Duke boundary conditions are applicable, which is the case for the valence-band envelope functions within a single-band model.

Burt[23] has also paid attention to the envelope functions for non-lattice-matched multilayer systems, but with a different approach. He uses his exact formulation of the envelope function method, but with a variable $\zeta(z)$ instead of z in the growth direction, so that in the coordinates (x,y,ζ) the unit cells of the strained multilayer lie on a Bravais lattice with a uniform period throughout. Therefore the boundary conditions that Burt deduces from his envelope function equations are the same for strained systems using the variable ζ and unstrained systems using z. Burt's boundary conditions do not explicitly include the lattice constant.

From Einevoll's boundary conditions we define two different state vectors for layer j. For holes we define

$$\chi_j^v(z) = \begin{bmatrix} \psi_j(z) \\ \dfrac{1}{m_j}\dfrac{d}{dz}\psi_j(z) \end{bmatrix} \qquad (2.6)$$

and for electrons in the conduction band we define

$$\chi_j^c(z) = \begin{bmatrix} \dfrac{1}{\mathbf{a}_j}\psi_j(z) \\ \dfrac{\mathbf{a}_j}{m_j}\dfrac{d}{dz}\psi_j(z) \end{bmatrix}, \qquad (2.7)$$

where $\mathbf{a}_j$ is the lattice constant.

The amplitude vector $\mathbf{U}_{j+1}$ of layer $j+1$ is related to that of layer j through the conditions for smooth joining, Eq. (2.5). Consequently, the amplitude vector of layer N is related to the amplitude vector of the zeroth layer by

$$\mathbf{U}_N = \mathbf{T}_{N,N-1} \cdot \mathbf{T}_{N-1,N-2} \cdot \cdots \cdot \mathbf{T}_{1,0} \cdot \mathbf{U}_0 = \mathbf{T} \cdot \mathbf{U}_0, \quad (2.8)$$

where $\mathbf{T}$ is a 2×2 matrix, derived in the Appendix. If N is the last layer of the structure, $\mathbf{T}$ is the total transfer matrix of the structure. Thus the amplitudes of the envelope wave function of each layer in the structure can be obtained without any preliminary assumptions about the number of layers, since $\mathbf{T}$ is obtained by a simple matrix multiplication.

2. Infinitely thick cap layer

For confined states ($E < V_B$) in a sample with infinitely thick capping we have the situation shown in Fig. 1(a). The confined eigenstates correspond to the zeroes of T_{00} (see the Appendix)

$$T_{00} = 0. \qquad (2.9)$$

For the unconfined states ($E > V_B$) in such sample structures the situation is as shown in Fig. 1(b), where we assume that the last (Nth) layer is infinitely wide. The energy levels for the unconfined above-barrier states correspond to the energies giving maxima in the transmission coefficient of the structure $|t|^2$, where t is given by (see the Appendix)

$$t = \frac{\det(\mathbf{T})}{T_{11}}. \qquad (2.10)$$

3. Finite cap layer

If the last layer in the structure (the cap layer) is of finite thickness and terminated by a finite vacuum potential [V_V in Fig. 1(c)], we can still use the $T_{00} = 0$ condition for the confined states, with an additional matrix multiplication for the total transfer matrix due to the additional ''vacuum layer.'' The above description for the above-barrier states, which now are semiconfined and not unconfined, needs to be modified for the structure with finite capping. We define a coefficient $|p|^2$ (see the Appendix) where p is given by

$$p = -\frac{\det(\mathbf{T})}{T_{01}}, \qquad (2.11)$$

and the maxima of this coefficient correspond to the above-barrier states in this case. The above-barrier states in our structures are calculated using this coefficient.

TABLE I. Sample parameters for the In$_x$Ga$_{1-x}$As/GaAs MQW's obtained by RHEED and HRXRD measurements. The well widths (L_W) and barrier widths (L_B) are in nm. All samples consist of four periods, except for 8 and 11 which have six periods in the MQW. Sample 11 has a $L_C = 80$ nm thick capping and the rest of the samples have a capping of the same thickness as the barriers ($L_C = L_B$). Also listed is the value of $x(x_{fit})$ obtained from a best fit between theory (using layer widths from the HRXRD) and experiment, and the energy (in eV) of PL line for the MQW's at 10 K.

	RHEED			HRXRD			Fit	PL
Sample	L_W	L_B	x_{RHEED}	L_W	L_B	x_{HRXRD}	x_{fit}	11H
1	15	40	0.095	15.3	42.7	0.100	0.106	1.409
2	15	20	0.095	14.6	20.6	0.104	0.113	1.403
3	15	10	0.095	14.8	10.5	0.099	0.105	1.411
4	15	5	0.095	15.4	5.5	0.093	0.099	1.417
5	5	40	0.090	5.0	40.7	0.087	0.086	1.464
6	5	30	0.095	4.7	27.2	0.120	0.123	1.442
7	5	40	0.095	4.7	36.4	0.100	0.113	1.449
8	5	35	0.095	4.4	30.5	0.100	0.105	1.458
9	5	50	0.095	4.5	45.1	0.095	0.098	1.461
10	5	60	0.095	5.2	63.4	0.085	0.082	1.468
11	5	35	0.105	5.2	35.9	0.100	0.100	1.457

III. EXPERIMENTAL DETAILS

A. Samples

All samples investigated in this study are In$_x$Ga$_{1-x}$As/GaAs MQW's with four or six periods and a nominal indium content of $x_{nom} = 0.1$. Buffer, wells, barriers, and cap layer are all nominally undoped. All substrates are n doped to $(1-4) \times 10^{18}$ cm^{-3}, except those for the $L_W \sim 15$ nm samples, which are semi-insulating. The sample parameters listed in Table I were obtained using both reflection high-energy electron diffraction (RHEED) and high-resolution x-ray diffraction (HRXRD) measurements.

The HRXRD measurements were performed using a Philips PW 1880 diffractometer using Cu $K\alpha$ radiation and a four-crystal Ge monochromator. The HRXRD spectra were recorded for the (004) reflection and the measured rocking curves were compared with simulated spectra to extract the MQW period and indium content. We estimate an uncertainty in the simulation results of 0.1 nm in the layer widths. The uncertainty is largest for the narrow well samples, because of the short period and weak HRXRD signal from these samples. For most samples the indium content ($0.08 \lesssim x_{XRD} \lesssim 0.12$) was found to be close to x_{nom}.

From Table I we see that the HRXRD values vary much more than the RHEED values and that the values of x_{XRD} vary with the energy of the MQW photoluminescence (PL) line (also listed in Table I) as expected: for two MQW's with the same well width (e.g., samples 6 and 7), the sample with lowest PL energy has the highest indium content. The PL line shifts with x together with the strained In$_x$Ga$_{1-x}$As band gap. In the calculations we use the HRXRD values for the layer widths and use x as a fitting parameter.

B. Experimental setup

We used a conventional PLE setup with a tunable Schwartz Electro-Optics Ti:sapphire laser as excitation

source, a SPEX 14018 double monochromator with 0.85-m focal length and 1800 grooves/mm gratings, and a Peltier-cell cooled RCA C31034 head-on GaAs photomultiplier tube in a photon counting mode. The samples were cooled down to 11 K using a Leybold ROK 10-300 closed-cycle cryostat, where the samples were mounted with colloidal silver on the cold finger. The detector was normally set to the photon energy of the excitonic transition between the first electron and heavy-hole level (11H) of the MQW when the PLE spectra were recorded. The wavelength calibration of the laser excitation was checked with an Advantest TQ8325 wavelength meter at the start of each PLE spectrum.

Polarized PLE was performed on some of the samples to distinguish transitions involving light holes and heavy holes. The samples were excited by light polarized parallel or normal to the sample surface. The excitation with normally polarized light was achieved by exciting the edge of the sample (90° angle of incidence), and luminescence escaping from the same edge was collected and detected. In this case the heavy-hole transitions are forbidden, and the PLE spectra will be dominated by transitions involving light holes. We also excited the sample with p-polarized light at an angle of incidence of 45°, where most of the light propagating in the sample will be polarized parallel to the layers, but a small fraction will be polarized normal to the layers. In this case, compared to excitation along the normal (0°), the intensity of transitions involving light holes will be enhanced, relative to the heavy-hole transitions.

IV. RESULTS FROM EXPERIMENTS

A. PL and PLE spectra

In Fig. 2 we show typical PLE spectra for four In$_x$Ga$_{1-x}$As/GaAs MQW's (samples 1–4) at 11 K with the same nominal well width ($L_W \simeq 15$ nm) but different barrier widths ($L_B \simeq 5$ to 40 nm). The laser excitation was at normal incidence. The detector energy position when recording the PLE spectra was set on the low-energy side of the 11H PL peak. The PL spectrum of one of the samples is shown as well in Fig. 2, and the linewidth of the 11H PL peak was found to be ~1 meV. We see from the figure that the difference in the energy position of the 11H peak in PL and PLE, the Stokes shift, is small (less than 1 meV), which indicates low disorder.[24] In this paper we will concentrate on the PLE spectra only, and no PL spectra will be discussed further.[25]

The PLE spectra show several peaks at energies both below and above the GaAs free-exciton line at 1.5153 eV (dashed line labeled GaAs FX in the figure). The energy position of this peak is well known and can be used to check the laser calibration. When we adjust for the differences in the 11H PL peak position caused by small deviations in the potential profile, we see that most peaks are at the same energy positions, i.e., the separation of most peaks and the 11H peak is the same for all four samples. However, we also see that steplike features in the spectra at energies close to the GaAs FX shift to higher energy when the barrier width decreases. This is seen more clearly in the insert of Fig. 2 where we have plotted three of the PLE spectra with the energy scale adjusted so that the origin is the energy position of the 11H peak for each sample.
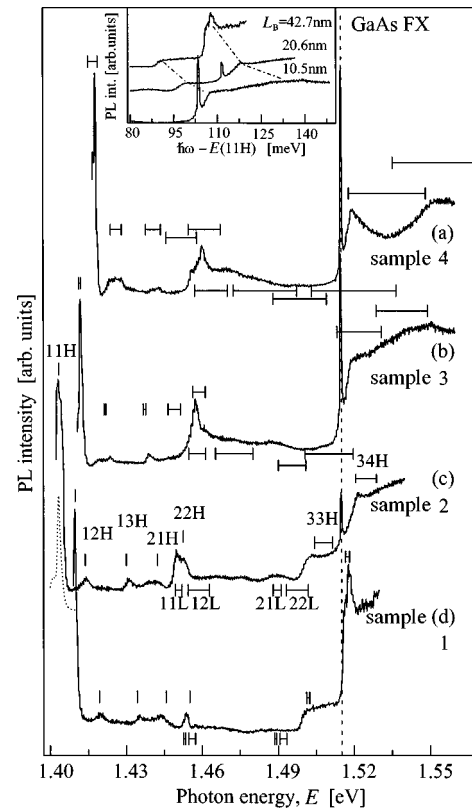

FIG. 2. PLE spectra for four different In$_x$Ga$_{1-x}$As/GaAs MQW's with the same well width $L_W \simeq 15$ nm, but different barrier widths $L_B = 5.5$ nm (a), 10.5 nm (b), 20.6 nm (c), and 42.7 nm (d). For sample 2 (c) the MQW ground-state PL (dotted line) is also shown. The dashed line indicates the energy position of free excitons in bulk GaAs (labeled GaAs FX). The spectra are normalized with respect to the 11H intensity and are shifted vertically for clarity. The lines and the horizontal bars are calculated transition energies, and the length of the horizontal bar indicates the (unbroadened) energy width of each transition. The peaks are labeled according to the calculations and the LH character of the corresponding peaks has been confirmed by polarized PLE. In the insert spectra (b), (c), and (d) are shown, on an energy scale relative to the 11H PLE transition.

In Fig. 3 we show high-resolution PLE spectra for energies around the GaAs FX energy (dashed line) for several samples with nominal well width $L_W \simeq 5$ nm, but different barrier widths ($L_B \simeq 30-60$ nm). The detector energy positions for these PLE recordings were set to be on the energy of the 11H PL transition and the laser excitation energy was stepped with 70 μeV (100 μeV for sample 8). The angle of incidence for the laser excitation was 45° for all spectra. All PLE spectra in Fig. 3 show a peak just above the GaAs buffer exciton. The peak is asymmetric and has highest intensity at the lower energies, in agreement with our results presented in Ref. 26. We see from the figure that the above-barrier peaks for the $L_W \simeq 5$ nm MQW's also shift towards higher energy with decreasing barrier width. We also see that the width of the peaks increases when the barrier widths decrease. All the samples in Fig. 3 have a cap layer that is of the same width as the barriers in the MQW, except for the sample with $L_B = 35.9$ nm [Fig. 3(e)] which has a $L_C = 80$-nm-thick capping. In the PLE spectrum for this sample we see an additional peak (indicated by the arrow
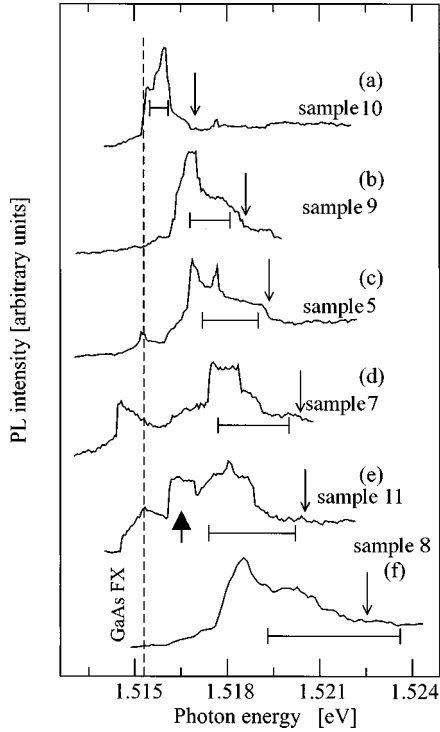
FIG. 3. PLE spectra for six samples with $L_W \simeq 5$ nm, but different barrier widths; $L_B = 63.4$ (a), 45.1 (b), 40.7 (c), 36.4 (d), 35.9 (e), and 30.5 (f) nm. The dashed line indicates the energy position of free excitons in bulk GaAs (labeled GaAs FX). The horizontal bars indicate calculated transition energies: the bar starts (ends) at the energy for transitions involving the first (last) subband level in the transition. The arrow with closed head points at transitions involving electrons and holes in the cap layer. The other arrows indicate the transition energies that result from use of the constructive interference condition.

FIG. 4. Logarithmic plot of the coefficient $|p|^2$ for a (In$_{0.1}$Ga$_{0.9}$As/GaAs) MQW calculated using three different sample structures, with $L_W = 15$ nm and $L_B = 20$ nm: Sample model with infinitely thick capping (i), sample model with finite cap-layer width but infinite vacuum potential (ii), and sample model with finite cap layer and vacuum barrier (iii). The dashed line (iv) is $|\sin(k_b L_B)|$ for $L_B = 20$ nm. The calculations in this paper are performed using the sample structure with finite capping and finite vacuum barrier.

assume that the exciton binding energy for above-barrier state transitions is close to, but still larger than, the value for excitons in bulk. In the calculation we used an exciton binding energy of $E_{exc} = 5$ meV for all transitions involving only above-barrier states. The light-hole exciton binding energies are taken to be 66% of the heavy-hole binding energies, from the differences in the reduced effective masses (we assume hydrogenlike binding).

V. RESULTS FROM CALCULATIONS

In this section we show how the energy levels of above-barrier states depend on the sample structure in general, as well as the calculated transition energies and overlap integrals for the particular In$_x$Ga$_{1-x}$As/GaAs MQW's that we have investigated by PLE.

A. General results

1. Potential profile and band offset

Due to the difference in lattice constant of In$_x$Ga$_{1-x}$As and GaAs, the In$_x$Ga$_{1-x}$As layers in our samples will sustain a biaxial compression. The main effects of this compressive strain is that the overall band gap is increased, and that the degeneracy of the valence-band edge is lifted. These effects will show up in the electrostatic potential profile of the MQW sample.

The potential profiles of our samples were calculated using the absolute energy positions of the band edges (taken from model-solid theory) in the two materials, with the strain induced shifts included.[29] We calculated well depths as a function of indium content and found that light holes were confined in the GaAs layers (type II) for $x \lesssim 0.17$. From the well depths we calculated the conduction-band offset Q_c, and the parabolic fit to the calculated Q_c gave the expression $Q_c = (64.9 - 9.6x - 1.6x^2)\%$.

with closed head in Fig. 3) between the GaAs FX and the above-barrier peak shifting with barrier width.

B. Exciton binding energies

For the samples where the band-to-band 11H step in the PLE spectra is clearly resolved we extract the exciton binding energy as the energy difference between the excitonic peak and the band-to-band step. For an In$_x$Ga$_{1-x}$As/GaAs MQW ($x \simeq 0.10$) with well width $L_W \simeq 15$ nm (5 nm) and $L_B \simeq 40$ nm barrier width we determine the heavy-hole exciton binding energy E_{exc} to be 6.5 ± 1 meV (9 ± 1 meV). This agrees well with what others have found through experiment or calculations.[27,28] We assume that these (confined state) exciton binding energies are correct also for the other samples with $x \simeq x_{nom}$ and approximately the same well width.

In our calculations we use the same E_{exc} for all transitions involving only confined states in the $L_W \simeq 15$ nm samples. For the parity forbidden transitions this will result in transition energies that are slightly too small, since E_{exc} is reduced when the overlap of the electron and hole wave functions is reduced. For the transitions involving carriers (semi)confined in different layers we assume that the exciton binding energy is smaller than that for the confined states, due to the smaller overlap of the electron and hole wave functions. We also
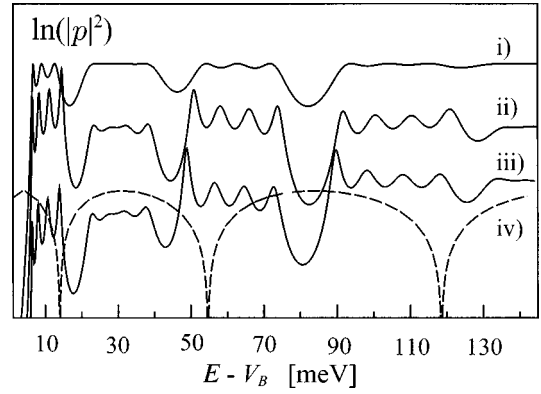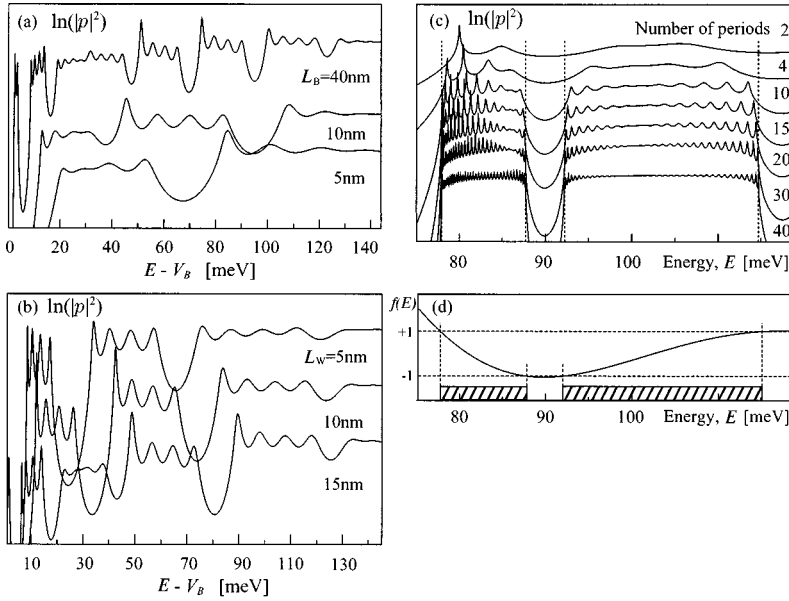
FIG. 5. Logarithmic plot of the coefficient $|p|^2$ for four different $(In_{0.1}Ga_{0.9}As/GaAs)$ MQW's with different barrier widths ($L_B = 5$, 10, and 40 nm, $L_W = 15$ nm) (a) and different well widths ($L_W = 5$, 10, and 15 nm, $L_B = 20$ nm) (b). In (c) we show $|p|^2$ for a MQW with increasing number of periods from top to bottom ($x = 0.1$, $L_B = 15$ nm, $L_W = 25$ nm), and in (d) we plot $f(E)$ for a superlattice with the same parameters. $f(E)$ is defined in the text.

2. Above-barrier states

As explained in Sec. II A 3 we use the maxima of the coefficient $|p|^2$, max($|p|^2$) where p is given in Eq. (2.11), to determine the energy levels of the above-barrier states. In Fig. 4 we show $|p|^2$ for three different sample structures of a $In_xGa_{1-x}As/GaAs$ MQW with four wells: a sample structure with an infinitely thick cap layer (i), a structure with finite cap layer thickness, but infinitely high vacuum potential barrier (ii), and finally, the structure used in the rest of this paper: with finite cap layer width and finite vacuum barrier (iii). Also shown in Fig. 4 is $|\sin(k_bL_B)|$ for $L_B = 20$ nm [(iv), dashed line]. Capizzi et al.[13] used the constructive interference condition [$\sin(k_bL_B) = 0$] to estimate the energy levels for the above-barrier states and found that it yields too high energies. Figure 4 shows that the peaks of the coefficient $|p|^2$ occur at lower energies than where $\sin(k_bL_B) = 0$, i.e., max($|p|^2$) yield results closer to the experimental values than $\sin(k_bL_B) = 0$.

In Fig. 5 we show the calculated coefficient $|p|^2$ for a MQW with four wells and finite cap-layer width, for three different barrier (a) or well (b) widths. We see from Fig. 5(a) that the above-barrier states behave much in the same way as confined states: $|p|^2$ shows bands consisting of four peaks (sublevels) as a consequence of the existence of four equal barriers in the structure (including the cap layer with $L_C = L_B$). Wide barriers yield energy levels just above the top of the barrier. In the same way the above-barrier bands of the MQW widen when the coupling between the barriers increases, as shown in Fig. 5(b).

Figure 5(c) shows how $|p|^2$ changes when the number of periods N in the MQW increases. In each band there are N peaks (if $L_C = L_B$), and we see that the bands widen with increasing N. In Fig. 5(d) we show, as a function of energy, the right-hand side [$f(E)$] of the equation defining the allowed energies in a superlattice:

$$\cos(qd) = \cos(k_WL_W)\cos(k_BL_B)$$
$$- \frac{1}{2}\left(\frac{k_B}{k_W} + \frac{k_W}{k_B}\right)\sin(k_WL_W)\sin(k_BL_B), \quad (5.1)$$

where q is a wave vector, $d = L_W + L_B$ is the superlattice period, and $k_{W,B}$ are given by

$$k_{W,B} = \sqrt{2m_{W,B}(V_{W,B} - E)/\hbar^2}$$

for the well (W) and barrier (B) layers. The allowed energy bands are those that give $-1 < f(E) < 1$, and are indicated by the hatching in Fig. 5(d). Going back to the $|p|^2$ for MQW's with increasing number of periods, we see that for $N \gtrsim 30$ the bandwidths of the MQW equal the superlattice bandwidths, and the MQW can be treated as a superlattice.

3. Inclusion of a_j in the boundary conditions

The inclusion of the lattice constant in the boundary conditions for conduction-band states shifts the energy levels of the confined states towards lower energies. For samples with low indium content and wide wells the difference in lattice constant is small, and the shift in energies is less than a fraction of a meV, as shown in Table II. In the table we list transition energies calculated[30] for three different samples with parameters taken from Ref. 31, with the lattice constant included and not included in the boundary conditions in columns labeled respectively, A and B. We see from the table that, in both cases, we get a very good agreement with experimental values taken from Ref. 31, for transitions involving both light holes and heavy holes, for $0.05 < x < 0.26$.

The choice of boundary conditions is therefore more important for samples with large indium contents ($x \gtrsim 20\%$) and narrow wells, where the shifts can be several meV.[32] Such a shift in the electron energy level will manifest itself in a reduced transition energy, and if the indium content is used as a fitting parameter a slightly too large indium content will result: for compositions around 0.3, for example, a shift in transition energy of 5 meV towards lower energy corresponds to a (fitted) indium content that is 0.007 too high, if the lattice constant is not included in the boundary conditions (for a MQW with $L_W = 3$ nm and $L_B = 50$ nm).

TABLE II. Transition energies for In$_x$Ga$_{1-x}$As/GaAs MQW's with $x<0.1$ or $x>0.2$. We list measured transition energies (Expt.) taken from Ref. 31 and our calculated transition energies (Theory) for the same sample structures. The choice of exciton binding energies is explained in the text. Column A (B) shows the results we get when the lattice constant is (is not) included in the boundary conditions.

$L_W/L_B/x$	15/80/0.073			10/80/0.206			9/80/0.253		
Transition	Expt.	Theory		Expt.	Theory		Expt.	Theory	
		A	B		A	B		A	B
11H	1.4465	1.4465[a]	1.4466[a]	1.3234	1.3234[c]	1.3243[c]	1.283	1.283[e]	1.2844[e]
12H	1.4563	1.4553[a]	1.4555[a]	1.3496	1.3446[c]	1.3455[c]			
13H	1.4698	1.4681[a]	1.4685[a]						
22H	1.4857	1.4858[a]	1.4860[a]	1.4263	1.4210[c]	1.4223[c]	1.411	1.4028[e]	1.4048[e]
11L	1.4764	1.4755[b]	1.4756[b]	1.4025	1.4012[d]	1.4021[d]	1.379	1.3769[f]	1.3783[f]

[a]$E_{exc}=5.2$ meV.
[b]$E_{exc}=2.7$ meV.
[c]$E_{exc}=4.3$ meV.
[d]$E_{exc}=1.8$ meV.
[e]$E_{exc}=3.3$ meV.
[f]$E_{exc}=0.8$ meV.

B. $|\psi|^2$ and transition energies for In$_x$Ga$_{1-x}$As/GaAs MQW's

We present here results from calculations of transition energies that are to be compared with those measured by PLE. We show two sets of results, for confined and above-barrier states. The former can be used to evaluate the agreement between theory and experiment in a wide energy range, and thereby support, or not, our calculational method for the above-barrier states.

1. $L_W \sim 5$ nm samples

In Fig. 6(a) we show $|\psi|^2$ for the two first electron levels (with sublevels) in a $L_W \sim 5$ nm sample with six wells. The interfaces between the layers are indicated by the dashed lines and the sample/vacuum interface is indicated by the dash-dotted line. The wells are the narrower layers in the figure. For these well widths there is only one confined level for electrons, and en $n>1$ is therefore an above-barrier state. We see from Fig. 6(a) that the $|\psi|^2$ is larger in the barriers than in the wells for the above-barrier state e2. An electron in an above-barrier state will therefore have a larger probability of being in the barrier than in the well. The distribution of $|\psi|^2$ is similar for heavy-hole confined and above-barrier states.

In Fig. 7 we show the calculated transition energies (solid lines) as a function of indium content, for two sets of In$_x$Ga$_{1-x}$As/GaAs MQW's with $L_W=5$ nm (a) or $L_W=4.5$ nm (b) and $L_B=30$, 40, or 60 nm (one line per transition and barrier width). The transitions are labeled nmH(L) for transitions involving the nth electron level and the mth heavy hole (light-hole) level. Electrons and heavy holes have only one confined level in the $L_W \sim 5$ nm samples. The 1mH and n1H, $n,m>1$, transitions will therefore involve one confined and one above-barrier state, and as these states have largest $|\psi|^2$ in different layers (see Fig. 6), we denote these transitions ''spatially indirect.'' In the calculations we assumed exciton binding energies of E$_{exc}=9$, 7, 5, and 6 meV for the 11H, 12H, 22H, and 11L transitions, respectively. We see from the figure that all transition energies decrease with increasing indium content, mainly due to the decrease in the strained In$_x$Ga$_{1-x}$As band gap. The dependence on the indium content is strongest for the transitions involving the lowest energy levels, and we see that the change in transition energy for the transition involving only above-barrier states (22H) is very small. From Fig. 7 we see that the dependence of the barrier width is strongest for the transitions involving higher-lying energy levels, as expected.

Also shown in Fig. 7 (the points) are the transition energies we measured for a set of $L_W \simeq 5$ nm In$_x$Ga$_{1-x}$As/GaAs MQW's (samples 5, 6, 8, 10, and 11). In the inserts of Fig. 7 we list the sample parameters found by HRXRD. Three of the samples have L_W near 5 nm and two of them have L$_W$ near 4.5 nm. The measured transition energies are positioned at the indium content that gave the best fit in the calculations of the 11H transition using the well widths listed in the inset of Fig. 7. A variation of the 11H exciton binding energy with ± 1 meV will result in a change in the fitted value of x by ∓ 0.002. The horizontal bars indicate the indium content found by HRXRD, and we see that the agreement is good between the values of x found by HRXRD and found through fitting the 11H transition energy. The difference between the two values of x are no larger than 0.005 for any sample in the set.

The results from our transition energy calculations for the 22H above-barrier transitions in the $L_W \simeq 5$ nm MQW's are indicated with horizontal bars in Fig. 3. The horizontal bars in that figure are not error bars, but indicate the spectral range of the transition: they start at the transition energy involving the lowest electron and heavy-hole subbands within each energy band and end at the highest. Also shown, indicated by $\downarrow$'s in the figure, are the transition energies for the above-barrier states that result if the constructive interference condition $[\sin(k_b L_B)=0]$ is used to calculate the above-barrier energy levels.

2. $L_W \sim 15$ nm samples

The calculated transition energies are indicated with horizontal bars as well in Fig. 2 containing the PLE spectra of the $L_W \simeq 15$ nm In$_x$Ga$_{1-x}$As/GaAs MQW's. The bars for the
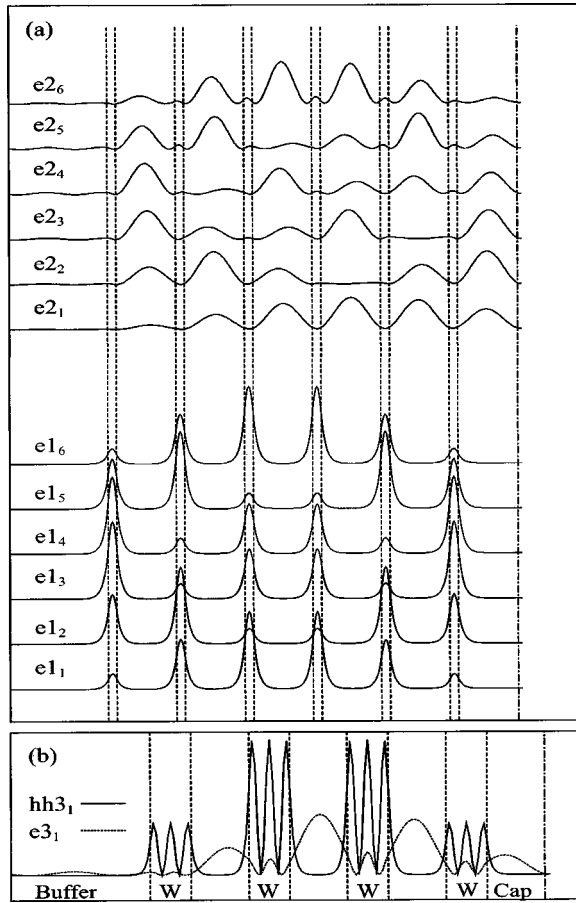
FIG. 6. $|\psi|^2$ for the first two electron levels e1 and e2 (with sublevels) in sample 8 ($L_W = 4.4$ nm, $L_B = 30.5$ nm, six wells) (a) and for the first sublevel of e3 and hh3 in sample 2 ($L_W = 14.6$ nm, $L_B = 20.6$ nm, four wells) (b). The electron and heavy-hole sublevels are labeled en_i and hn_i, respectively, where n is the level index and i the sublevel index. The dashed lines indicate the interfaces between the layers, and the dash-dotted lines the interface between the sample and vacuum. The last layer to the right is the cap layer.

transitions involving heavy holes are drawn just above the measured PLE spectra and those involving light holes are below. Again the horizontal bars start (end) at the transition energy involving the lowest (highest) electron and hole subbands within each energy band. For the wide barrier samples, the width of the low-energy transitions is not resolved and the horizontal bar for these transitions degenerates into a vertical line. Only the transitions for the $L_B \simeq 20.6$ nm MQW (sample 2) are labeled, but it is the same transitions that are indicated for all samples. All four samples in the figure have two confined electron levels and three confined heavy-hole levels. The 33H transition is therefore a spatially indirect transition where the electrons are semiconfined in the GaAs barriers and the heavy holes are confined in the In$_x$Ga$_{1-x}$As wells, as shown in Fig. 6(b).

In Table III we list the calculated transition energies for some of the samples that we showed PLE spectra from in Figs. 2 and 3. The overlap integrals of the electron and hole envelope functions involved in the transitions are also listed in Table III. All envelope functions are normalized over the whole sample structure, including a 500-nm-thick buffer layer, N wells, $N-1$ barriers ($N = 4$ or 6), capping, and 2 nm of the vacuum.
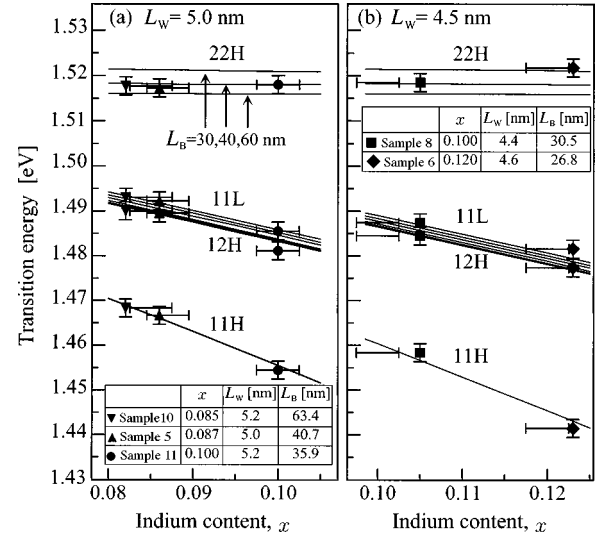

FIG. 7. Calculated transition energies (lines) for In$_x$Ga$_{1-x}$As/GaAs MQW's as a function of indium content, for three different barrier widths $L_B = 30$, 40, or 60 nm and well width $L_W = 5$ nm (a) and $L_W = 4.5$ nm (b). Transition energies measured by PLE (at 11 K) are indicated by symbols and the horizontal bars indicate the indium content found by HRXRD for each sample. In the insets we list the sample parameters found by HRXRD. The measured transition energies are positioned at the indium content that gives the best fit for the 11H transition for the well widths measured by HRXRD.

VI. DISCUSSION

A. Transition energies for In$_x$Ga$_{1-x}$As/GaAs MQW's

1. $L_W \sim 5$ nm samples

We start the discussion of the results for the actual samples by comparing the measured and calculated transition energies for the $L_W \sim 5$ samples shown in Fig. 7. We see from the figure that the calculated and measured 11H, 11L, and 22H transition energies agree well, when we adjust for the deviation from $L_W = 5$ and 4.5 nm: for narrower (wider) wells the energy levels will shift towards higher (lower) energies and we see that the points for the $L_W = 4.4$ nm sample lie above the $L_W = 4.5$ nm lines [see Fig. 7(b)]. Similarly, the points for the $L_W = 5.2$ nm samples are below the $L_W = 5$ nm lines [see Fig. 7(a)].

For the parity-forbidden 12H transition the agreement is very good for the $L_B = 63.4$ nm sample (10), and not so good for the rest. This is probably due to the choice of exciton binding energy we have made: we have used the same $E_{exc} = 7$ meV for all $L_W \sim 5$ nm samples. If we instead extract the exciton binding energy as the difference between the calculated band-to-band energies and the measured transition energies, we find that the exciton binding energy for the 12H transition increases from $\simeq 5$ meV to $\simeq 9$ meV when the barrier thickness decreases from 63.4 nm to 30.5 nm. For the sample with the narrowest barrier (26.8 nm) we estimate an exciton binding energy of $\simeq 5.5$ meV. This increase followed by a decrease in E_{exc} with decreasing barrier thickness is the same trend as for the 11H exciton binding energy with decreasing well thickness. Bastard, Mendez, Chang, and Esaki show in Ref. 33 that when the electron and hole are present in spatially separated regions (type II), the exciton binding

TABLE III. Calculated and experimentally observed transition energies for In$_x$Ga$_{1-x}$As/GaAs MQW's. The notation 12H (12L) means the transition between the first electron level and the second heavy- (light-) hole level. All energies are in eV, and are taken to be in the middle of the subbands, unless otherwise stated. The overlap integral of the envelope functions involved in the transitions are also listed. The full overlap integral is taken to have a value of 100. L_W and L_B are found through HRXRD and x is used as a fitting parameter. The fitted value of x is close to the HRXRD value (x_{XRD} in the table) for all samples. The values for transitions involving only above-barrier states are overlined, and they are underlined for those involving one above-barrier state.

Sample	1			2			8		
$L_W/L_B/x(x_{XRD})$	15.3/44.6/0.106(0.100)			14.6/20.6/0.113(0.104)			4.4/30.5/0.105(0.100)		
	Position			Position			Position		
Transition	Expt.	Theory	Overlap	Expt.	Theory	Overlap	Expt.	Theory	Overlap
11H	1.4100	1.4099[b]	98.9	1.4034	1.4035[b]	98.9	1.4584	1.4584[e]	94.6
12H	1.4200	1.4194[b]	1.3	1.4140	1.4138[b]	1.3	<u>1.4845</u>	<u>1.4844[e]</u>	<u>19.3</u>
13H	1.4355	1.4343[b]	11.2	1.4310	1.4300[b]	11.5			
21H	1.4440	1.4458[b]	1.2	1.4420	1.4424[b]	1.2			
22H	1.4540	1.4553[b]	94.5	1.4530	1.4526[b]	95.0	1.5185	1.5212[c]	91.2
33H[a]	<u>1.5015</u>	<u>1.5013[c]</u>	<u>25.0</u>	<u>1.5030</u>	<u>1.5050[c]</u>	<u>43.7</u>			
34H[a]	1.5168	1.5169[c]	61.2	1.5215	1.5210[c]	36.5			
11L	<u>1.4540</u>	<u>1.4531[d]</u>	<u>39.8</u>	<u>1.4500</u>	<u>1.4515[d]</u>	<u>57.5</u>	<u>1.4874</u>	<u>1.4870[f]</u>	<u>54.1</u>

[a]Onset of the transition.
[b]$E_{exc}=6.5$ meV.
[c]$E_{exc}=5.0$ meV.
[d]$E_{exc}=4.3$ meV.
[e]$E_{exc}=9.0$ meV.
[f]$E_{exc}=6.0$ meV.

energy is substantially reduced and lower than the bulk values. They assume, however, that the carriers are completely confined, which is not the case for the above-barrier states involved in the 12H transitions under discussion. Recently, several groups have calculated E_{exc} for type-II quantum structures, but to our knowledge there are no reports of calculated E_{exc} for transitions involving (semiconfined) above-barrier states.

As far as above-barrier transitions are concerned (PLE spectra and calculated transition energies just above the GaAs free exciton), Fig. 3 shows a generally very good agreement that is best for the widest barriers. This indicates that the exciton binding energy for the above-barrier transitions depends on the barrier width: if we again extract the exciton binding energy we find that for the $L_B \gtrsim 40$ nm samples, the above-barrier exciton binding energy is 5 meV and it increases to ~8 meV for the $L_B = 30.5$ nm sample. The good agreement between theory and experiment for the above-barrier states suggests that the condition max $(|p|^2)$ can be used successfully to calculate the above-barrier energy levels.

The full arrow in Fig. 3 indicates a calculated transition energy for a transition involving a hole with an envelope wave function that is larger in the cap layer than in the rest of the sample structure. In the calculations we found this kind of wave function for many samples, but in the samples with $L_C = L_B$ they appear as the topmost subband in each energy band. In the sample with a cap layer much wider than the barriers, the corresponding transition is pushed towards lower energies and we can resolve it clearly in the PLE spectrum. Huang[34] has treated cap-layer states in MQW's theo-

retically and he found that with increasing number of periods in the MQW, the full width at half-maximum (FWHM) of the cap-layer level decreases. The peak indicated by the arrow in the PLE spectrum of sample 11 in Fig. 3(e) has a FWHM of $\simeq 1$ meV. This value agrees well with Huang's calculated FWHM of the cap-layer electron state for a MQW with six periods.

2. $L_W \sim 15$ nm samples

The intensity of a peak in a PLE spectrum is proportional to the probability for the transition and therefore to the overlap integral of the electron and hole wave functions. When we compare the PLE spectrum in Fig. 2(d) with the calculated overlap integrals in Table III we see that the parity-forbidden transitions (nmH, $n \neq m$) are much stronger than what the value of the overlap integral suggests. A possible explanation for this deviation could be the fact that we have used a rectangular potential profile in our calculations, instead of the trapezoidal shape one expects to find in MBE-grown In$_x$Ga$_{1-x}$As/GaAs MQW's due to indium segregation.[35] Lambkin et al. show in Ref. 36 that the breakdown of the normal $\Delta n = n - m = 0$ selection rule is not caused by any built-in electric field and suggest that random fluctuations in the alloy or large-scale variations in the indium content due to indium segregation are causing the breakdown. A trapezoidal potential profile will break the symmetry, and thereby the selection rules for the transitions, and the overlap of the wave functions can be larger for "nmH, $n \neq m$" transitions.

Asymmetry is also introduced by the sample being terminated close to the MQW region. We observe that this latter asymmetry is important only when the vacuum is very close to the wells, i.e., for thin cap layers $L_C \lesssim 20$ nm. In the samples where the forbidden transitions show up (see Fig. 2), the thickness of the cap layer lies on both sides of this value, ranging from 5 to 40 nm. Therefore, we conclude that the forbidden transitions are not due to asymmetry caused by the proximity of the sample termination. Another source for some discrepancy between the calculated overlap integrals and the observed peak intensities could be that a single-band model has been used in the calculations. This model neglects the valence-band mixing that can influence the wave functions, even if the energies are correct at the zone center. However, in our samples we believe this effect to be negligible because of the very large (several tens of meV) splitting between the heavy-hole and light-hole band edges. The parity-forbidden transitions have been observed by several other groups too; see, for example, Reithmaier et al.[37] and Joyce et al.[38]

We have also calculated the probability of finding the carrier in the MQW region (including capping) and in the buffer. These probabilities oscillate with increasing the energy above the barrier, as Fafard et al. have shown in Ref. 39. The amplitude of the maxima in the (oscillating) probability of finding the particle in the MQW region decreases when the energy increases, and finally the carrier will have a larger probability of being in the buffer (when the buffer is much wider than the MQW region). This explains why we observe only transitions involving the first unconfined above-barrier states.

Ksendzov, Pike, and Larsson show in Ref. 40 that interband transitions between confined and unconfined states in quantum wells give rise to slow-onset absorption features (steps). The 33H transitions in the PLE spectra in Figs. 2(b), 2(c), and 2(d) are indeed slow-onset steplike features, so our interpretation of the PLE spectra indicated by the labels on the peaks in the figure, is justified. From the inspection of Fig. 2 we conclude that the calculated transition energies involving both confined and above-barrier states agree very well with the measured ones, especially for the wide barrier samples.

VII. SUMMARY AND CONCLUSIONS

We have used the effective-mass approximation in a transfer-matrix formalism to calculate the energy levels and envelope wave functions of both confined and above-barrier states in $In_xGa_{1-x}As/GaAs$ MQW's. We have formulated a condition, max $(|p|^2)$ where p is expressed by the transfer-matrix elements, that is satisfied for energies corresponding to the semiconfined above-barrier levels in the case of a finite cap layer. We have used the envelope wave function boundary conditions deduced by Einevoll et al. for strained systems, and have shown that the energy levels can be significantly shifted compared to the case of the BenDaniel-Duke boundary conditions. We have compared calculated transition energies with measured ones for several MQW's and we find a good agreement between theory and experiment, for transitions involving confined as well as above-barrier states.

APPENDIX: TRANSFER MATRICES

The state vector for electrons can be written

$$\chi_j(z) = \mathbf{M}_j^c(z) \cdot \mathbf{U}_j, \tag{A1}$$

where $\mathbf{U}_j$ is the amplitude vector for the envelope wave function in layer j defined by Eq. (2.2) and

$$\mathbf{M}_j^c(z) = \begin{bmatrix} \dfrac{1}{\mathbf{a}_j}\exp[k_j(z-z_j)] & \dfrac{1}{\mathbf{a}_j}\exp[-k_j(z-z_j)] \\ \dfrac{\mathbf{a}_j \cdot k_j}{m_j}\exp[k_j(z-z_j)] & \dfrac{-\mathbf{a}_j \cdot k_j}{m_j}\exp[-k_j(z-z_j)] \end{bmatrix}. \tag{A2}$$

The state vector for holes can also be written as in Eq. (A1), but with $\mathbf{M}_j^v(z)$, given by

$$\mathbf{M}_j^v(z) = \begin{bmatrix} \exp[k_j(z-z_j)] & \exp[-k_j(z-z_j)] \\ \dfrac{k_j}{m_j}\exp[k_j(z-z_j)] & \dfrac{-k_j}{m_j}\exp[-k_j(z-z_j)] \end{bmatrix}, \tag{A3}$$

instead of $\mathbf{M}_j^c(z)$.

With these notations the conditions for smooth joining can be expressed as

$$\mathbf{M}_{j+1}(z_{j+1}) \cdot \mathbf{U}_{j+1} = \mathbf{M}_j(z_{j+1}) \cdot \mathbf{U}_j, \tag{A4}$$

with $\mathbf{M} = \mathbf{M}^c$ or $\mathbf{M}^v$ for electrons and holes, respectively. By multiplying each side of Eq. (A4) by the inverse of $\mathbf{M}_{j+1}(z_{j+1})$ we get

$$\mathbf{U}_{j+1} = \mathbf{M}_{j+1}^{-1}(z_{j+1}) \cdot \mathbf{M}_j(z_{j+1}) \cdot \mathbf{U}_j = \mathbf{T}_{j+1,j} \cdot \mathbf{U}_j, \tag{A5}$$

where $\mathbf{T}_{j+1,j}$ is the 2×2 transfer matrix that relates the amplitude vector of layer $j+1$ to that of layer j. The amplitude vector of layer N is related to the amplitude vector of the zeroth layer by

$$\mathbf{U}_N=\mathbf{T}_{N,N-1}\cdot\mathbf{T}_{N-1,N-2}\cdot\ \cdots\ \cdot\mathbf{T}_{1,0}\cdot\mathbf{U}_0=\mathbf{T}\cdot\mathbf{U}_0,\quad\text{(A6)}$$

or

$$\begin{bmatrix}U_N^R\\U_N^L\end{bmatrix}=\begin{bmatrix}T_{00}&T_{01}\\T_{10}&T_{11}\end{bmatrix}\begin{bmatrix}U_0^R\\U_0^L\end{bmatrix}.\quad\text{(A7)}$$

If N is the last layer of the structure, $\mathbf{T}$ is the total transfer matrix of the structure. Thus the amplitudes of the envelope wave function of each layer in the structure can be obtained without any preliminary assumptions about the number of layers, since $\mathbf{T}$ is obtained by a simple matrix multiplication.

a. Infinitely thick cap layer. For confined states ($E<V_B$) we have the situation shown in Fig. 1(a). In the zeroth layer the envelope wave function is

$$\psi_0=U_0^R\exp(k_0z),\quad z<0;\quad\text{(A8)}$$

and in the Nth layer it is

$$\psi_N=U_N^L\exp[-k_N(z-z_N)],\quad z>z_N.\quad\text{(A9)}$$

From Eq. (A7) we get

$$\begin{bmatrix}0\\U_N^L\end{bmatrix}=\begin{bmatrix}T_{00}&T_{01}\\T_{10}&T_{11}\end{bmatrix}\begin{bmatrix}U_0^R\\0\end{bmatrix}=\begin{bmatrix}T_{00}U_0^R\\T_{10}U_0^R\end{bmatrix}.\quad\text{(A10)}$$

We see that to satisfy Eq. (A10) we must have

$$T_{00}=0.\quad\text{(A11)}$$

In other words, the confined eigenstates correspond to the zeroes of T_{00}.

For unconfined states ($E>V_B$) the situation is as shown in Fig. 1(b), where we assume that the last (Nth) layer is infinitely thick. An incoming wave from the left has amplitude $U_0^R=1$. A part of this wave is reflected at the MQW structure and the rest is transmitted. The amplitude of the reflected wave is r and t for the transmitted wave. r and t are of course the reflection and transmission coefficients. We now get the following equations for r and t:

$$\begin{bmatrix}t\\0\end{bmatrix}=\begin{bmatrix}T_{00}&T_{01}\\T_{10}&T_{11}\end{bmatrix}\begin{bmatrix}1\\r\end{bmatrix}=\begin{bmatrix}T_{00}+T_{01}r\\T_{10}+T_{11}r.\end{bmatrix}\quad\text{(A12)}$$

If we solve this for r and t we get

$$r=-\frac{T_{10}}{T_{11}},\quad\text{(A13)}$$

and

$$t=T_{00}+T_{01}r=\frac{\det(\mathbf{T})}{T_{11}}.\quad\text{(A14)}$$

If we plot $|t|^2$ as a function of energy, we will see that $|t|^2$ has sharp maxima for certain energies. If the first and last layer in the structure are of the same kind, i.e., $k_0(E)=k_N(E)$, we have that

$$|r|^2+|t|^2=1,\quad\text{(A15)}$$

and the maximum values of $|t|^2$ equals 1.

The energies where $|t|^2$ has its maxima are the energy levels of the resonant, above-barrier states for the quantum structure. Plots of $|\psi|^2$ for increasing carrier energies above the barrier reveal that for carriers with energy where $|t|^2$ has a maximum, $|\psi|^2$ is larger above the quantum structure than in the wide buffer. Therefore, an electron (or hole) in an above-barrier state is not confined to the quantum structure, but spends a longer time in the quantum structure than in the buffer layer.

For structures where the last layer has a higher potential than the zeroth (but still lower than the resonant energy), we find the resonant energy levels where $|t|^2$ has a maximum that generally does not equal unity.

b. Finite cap layer. If the last layer in the structure (the cap layer) is of finite width and terminated by a finite vacuum potential [V_V in Fig. 1(c)], the above description for the above-barrier states needs to be modified. We still have an incoming wave with an amplitude $U_0^R=1$ and $U_0^L=r$ in layer 0, as shown in Fig. 1(c). In the vacuum layer we can only have a left-going part of the envelope wave function

$$\psi_N(z)=U_N^L\exp[-k_N(z-z_N)]$$
$$=p\ \exp[-k_N(z-z_N)],\quad z>z_N,$$

thus

$$\begin{bmatrix}0\\p\end{bmatrix}=\begin{bmatrix}T_{00}&T_{01}\\T_{10}&T_{11}\end{bmatrix}\begin{bmatrix}1\\r\end{bmatrix}=\begin{bmatrix}T_{00}+T_{01}r\\T_{10}+T_{11}r\end{bmatrix}\quad\text{(A16)}$$

If we solve this for r and p we get

$$r=-\frac{T_{00}}{T_{01}}\quad\text{(A17)}$$

and

$$p=T_{10}+T_{11}r=-\frac{\det(\mathbf{T})}{T_{01}}.\quad\text{(A18)}$$

This new coefficient p will also have its maxima for energy levels where $|\psi(z)|^2$ is largest above the quantum structure. The above-barrier states in our structures are calculated using this coefficient.

*Electronic address: worren@phys.ntnu.no

†Department of Electronic and Electrical Engineering, University of Sheffield, Mappin Street, Sheffield S1 3JD, United Kingdom. Electronic address: K.Ozanyan@sheffield.ac.uk

[1] J.E. Zucker *et al.*, Phys. Rev. B **29**, 7065 (1984).

[2] G. Bastard *et al.*, Solid State Commun. **49**, 671 (1984).

[3] K.B. Wong, M. Jaros, M.A. Gell, and D. Ninno, J. Phys. C **19**, 53 (1986).

[4] J.J. Song *et al.*, Phys. Rev. B **34**, 8958 (1986).

[5] U.K. Reddy *et al.*, J. Appl. Phys. **62**, 145 (1987).

[6] P.S. Jung *et al.*, Superlattices Microstruct. **4**, 581 (1988).

[7] H. Shen *et al.*, Solid State Commun. **65**, 929 (1988).

[8] S.H. Pan *et al.*, Phys. Rev. B **38**, 3375 (1988).

[9] G. Ji *et al.*, J. Appl. Phys. **62**, 3366 (1987); G. Ji, W. Dobbelaere, D. Huang, and H. Morkoç, Phys. Rev. B **39**, 3216 (1989).

[10] K.J. Moore, G. Duggan, A. Raukema, and K. Woodbridge, Superlattices Microstruct. **7**, 303 (1990); K.J. Moore, Ph.D. thesis, University of Twente, The Netherlands, 1991.

[11] F.C. Zhang *et al.*, Phys. Rev. Lett. **68**, 3220 (1992).

[12] F. Martelli *et al.*, Phys. Rev. B **48**, 1643 (1993).

[13] M. Capizzi *et al.*, Solid-State Electron. **37**, 641 (1994).

[14] G. Wen and Y.-C. Chang, Phys. Rev. B **49**, 16 585 (1994).

[15] B. Jogai and P.W. Yu, Phys. Rev. B **41**, 12 650 (1990).

[16] J. Leymarie *et al.*, Phys. Rev. B **51**, 13 274 (1995).

[17] G. Arnaud *et al.*, Phys. Rev. B **46**, 15 290 (1992).

[18] A.K. Ghatak, K. Thyagarajan, and M.R. Shenoy, IEEE J. Quantum Electron. **24**, 1524 (1988).

[19] J.-Th. Zettler *et al.*, Phys. Rev. B **46**, 15 955 (1992).

[20] See, for example, E. Merzbacher, *Quantum Mechanics*, 2nd ed. (Wiley International Edition, New York, 1970).

[21] An introduction to the envelope function approximation can be found in G. Bastard, *Wave Mechanics Applied to Semiconductor Heterostructures* (Les Éditions de Physique, Les Ulis, France, 1988).

[22] G.T. Einevoll, Phys. Rev. B **42**, 3497 (1990); G.T. Einevoll and L.J. Sham, *ibid.* **49**, 10 533 (1994).

[23] M.G. Burt, J. Phys. Condens. Matter **4**, 6651 (1992); M.G. Burt, in *Bandstructure Engineering in Semiconductor Microstructures*, Vol. 189 of *NATO Advanced Study Institute Series B: Physics*, edited by R.A. Abram and M. Jaros (Plenum, New York, 1989), p. 99.

[24] A. Polimeni *et al.*, Phys. Rev. B **54**, 16 389 (1996).

[25] The PL of similar samples grown in the same MBE chamber is presented in A. Patanè, A. Polimeni, M. Capizzi, and F. Martelli, Phys. Rev. B **52**, 2784 (1995); F. Martelli *et al.*, *ibid.* **53**, 7421 (1996).

[26] T. Worren, K.B. Ozanyan, F. Martelli, and O. Hunderi, Microelectron. Eng. **43-44**, 271 (1998).

[27] J.-P. Reithmaier, R. Höger, and H. Riechert, Phys. Rev. B **43**, 4933 (1991).

[28] R. Atanasov, F. Bassani, A. D'Andrea, and N. Tomassini, Phys. Rev. B **50**, 14 381 (1994).

[29] C.G. Van de Walle, Phys. Rev. B **39**, 1871 (1989).

[30] For the calculation of transition energies in Table II, we used the 11H exciton binding energy as a fitting parameter. We allowed the E_{exc} to vary with a few meV from 6.5 (7.5) meV for the $L_{\mathrm{W}}=15$ (10) nm samples. The 11L E_{exc} was adjusted with the same amount from 4.0 (5.0) meV for the $L_{\mathrm{W}}=15$ (10) nm samples. A shift in 11H of a few meV corresponds to a variation of x with ± 0.005, which is justified since in Ref. 31 the indium content is not a measured value.

[31] J.-P. Reithmaier *et al.*, Appl. Phys. Lett. **56**, 536 (1990).

[32] T. Worren, K.B. Ozanyan, F. Martelli, and O. Hunderi, Phys. Scr. **T69**, 336 (1996).

[33] G. Bastard, E.E. Mendez, L.L. Chang, and L. Esaki, Phys. Rev. B **26**, 1974 (1982).

[34] F.Y. Huang, Appl. Phys. Lett. **57**, 1669 (1990).

[35] See for example: J.M. Moison *et al.*, Phys. Rev. B **40**, 6149 (1989) or J.-M. Gerard and J.-Y. Marzin, *ibid.* **45**, 6313 (1992).

[36] J.D. Lambkin, L.K. Howard, and M.T. Emeny, Phys. Rev. B **42**, 1738 (1990).

[37] J.P. Reithmaier, R. Höger, H. Riechert, P. Hiergeist, and G. Abstreiter, Appl. Phys. Lett. **57**, 957 (1990).

[38] M.J. Joyce, Z.Y. Xu, and M. Gal, Phys. Rev. B **44**, 3144 (1991).

[39] S. Fafard, E. Fortin, and A.P. Roth, Phys. Rev. B **45**, 13 769 (1992); S. Fafard, *ibid.* **46**, 4659 (1992); S. Fafard, E. Fortin, and A.P. Roth, *ibid.* **47**, 10 588 (1993).

[40] A. Ksendzov, W.T. Pike, and A. Larsson, Phys. Rev. B **47**, 2228 (1993).